Catalysis Science & Technology

ROYAL SOCIETY OF CHEMISTRY

PAPER

View Article Online
View Journal | View Issue

Check for updates

Cite this: *Catal. Sci. Technol.*, 2024, **14**, 1923

Disordered medium-pore zeolite PST-24 as an efficient low-temperature isobutanol dehydration catalyst†

Jeong Hwan Lee, ‡[a] Donghui Jo [b] and Suk Bong Hong *[a]

Received 16th January 2024,
Accepted 21st February 2024

DOI: 10.1039/d4cy00063c

rsc.li/catalysis

The synthesis of PST-24 with a relatively high Al content (Si/Al = 47), a disordered medium-pore zeolite, using the seeding technique and its catalytic properties for the low-temperature (250 °C) dehydration of isobutanol to isobutene are presented. This PST-24 was found to be considerably more active and stable for isobutanol dehydration than H-ZSM-5 and H-ferrierite with similar Si/Al ratios, the two most widely studied catalysts for this reaction, revealing its high potential as a new dehydration catalyst for biomass-derived isobutanol. While variable-temperature IR spectroscopy with adsorbed isobutanol reveals stronger interactions of isobutanol molecules with the PST-24 framework than with the latter two zeolite frameworks, ^{1}H–^{13}C CP MAS spectroscopy shows the formation of soft coke only in the former catalyst.

Introduction

Isobutene is the most valuable component among the butene isomers because of a multitude of applications in various chemical industries.[1,2] An excellent example is its use in the production of isobutene–isoprene rubber, a synthetic polymer commonly known as butyl rubber that has high impermeability, excellent chemical resistance and great mechanical robustness and elasticity, thus being indispensable for the manufacture of numerous daily necessities, including tires, tubes and electrical insulators. While the majority of isobutene is currently produced by distillation of the C4 raffinate stream in a naphtha cracking unit, on the other hand, the implementation of a carbon tax for greenhouse gas emissions has prompted considerable research efforts to develop a viable alternative to this process. It was in the mid-2010s when Gevo commercialized the production of isobutanol from renewable bioresources like sugar, dextrose, lignin and cellulose using yeast biocatalysts.[3,4] Therefore, the dehydration of bio-based isobutanol can open an environmentally friendly pathway to isobutene.

A wide variety of solid acids, including amorphous silica-alumina, mixed-metal oxides and hydroxyapatites, have been investigated for alcohol dehydration so far.[5–9] Owing to its cost-effective availability, for example, γ-alumina has been extensively studied for isobutanol dehydration.[10–12] However, a significant decrease in dehydration activity by water is the serious drawback of this catalyst, despite its high selectivity toward isobutene:[12] at 285 °C, isobutanol conversion decreased from 53–61 to 28–42% upon co-feeding of 15 wt% water.[10]

On the other hand, aluminosilicate zeolites with channels and cavities of molecular dimensions have been of fundamental interest in the dehydration of isobutanol to isobutene, because of their well-known shape- and surface-selective properties. For example, de Reviere *et al.* examined the effect of zeolite framework topology on this reaction and showed that the proton form (H-ZSM-5) of the medium-pore high-silica (Si/Al = 24) zeolite ZSM-5 (framework type MFI) outperformed large-pore zeolites H-Y (FAU; Si/Al = 39) and H-mordenite (MOR; Si/Al = 11). Although the latter two catalysts showed negligible isobutanol conversion at 240 °C and 5 bar, the conversion over H-ZSM-5 was found to be *ca.* 50%, probably due to the optimal fit of isobutanol and reaction intermediates within its 10-ring channel intersections.[13] H-ferrierite (FER), a former industrial catalyst for the skeletal isomerization of *n*-butenes to isobutene,[14] was also reported to be highly selective for isobutanol dehydration to produce linear butenes.[15–17] This medium-pore zeolite exhibited similar activity in both the presence and absence of 10% water in the feed even after 15 h, except for a nominal decrease in isobutanol conversion (~10%) at early time on stream.[15]

[a] *Center for Ordered Nanoporous Materials Synthesis, Division of Environmental Science and Engineering, POSTECH, Pohang 37673, Korea. E-mail: sbhong@postech.ac.kr*
[b] *Low-Carbon Petrochemical Research Center, Korea Research Institute of Chemical Technology (KRICT), Daejeon 34114, Korea*
† Electronic supplementary information (ESI) available. See DOI: https://doi.org/10.1039/d4cy00063c
‡ Present address: Department of Chemical Engineering, The Pennsylvania State University, University Park, Pennsylvania 16802, United States.

PST-24 is a new disordered medium-pore zeolite synthesized via the so-called excess fluoride approach[18] using the pentamethylimidazolium (PMI^+) cation as an organic structure-directing agent (OSDA).[19] Its pore architecture is exceedingly unique in that the intracrystalline channel dimensionality varies locally from two-dimensional (2D) to bi-level 2D to 3D. While the composite cas-zigzag building chains in PST-24, which are connected by 'disordered' double 5-ring (d5r) columns, are ordered throughout the whole framework structure, the d5r column pairs can adopt two different arrangements that 'close' and 'open' 10-ring (6.1 × 3.5 Å) channels along the [101] direction as illustrated in Fig. 1. This has led us to suggest three representative ordered polytype structures, denoted as PST-24A ($P2_1/c$), PST-24B ($P\bar{1}$) and PST-24C ($P2/c$), where the second one is the alternating structure of the first and third ones.[19] Consequently, PST-24 has 10-ring pockets ($[4.5^6{\cdot}6^6{\cdot}8^2{\cdot}10]$ cages; PST-24A) and short 10-ring channels along [101] (PST-24C) (Fig. 1), in addition to parallel straight 10-ring (5.8 × 5.4 Å) and 8-ring (4.8 × 3.1 Å) channels along [010] and sinusoidal 8-ring channels along [001]. Such a pore structure provides the distinctive void space in the spectrum of medium-pore cavities where the channel intersections of ferrierite and ZSM-5 belong, rendering PST-24 attractive as an efficient isobutanol dehydration catalyst.

However, the lowest Si/Al ratio (or the highest Al content) of PST-24 that can be achieved by direct synthesis is about 200.[19] Such difficulty in incorporating more Al atoms into its framework, which is often observed in zeolite synthesis under normal fluoride conditions (HF/OSDA = 1.0),[20] can limit the potential of this disordered zeolite as a solid acid catalyst or catalyst support. Here we show that the Si/Al ratio of PST-24 can be lowered as low as 50 when 4 wt% of calcined PST-24 with Si/Al = 200 is added as seed crystals to a PMI^+-containing synthesis mixture. We also show that the proton form of this PST-24 zeolite is considerably more active and stable for the low-temperature (250 °C) dehydration of isobutanol to isobutene than H-ZSM-5 and H-ferrierite with similar Si/Al ratios. The origin of the high isobutanol reactivity of H-PST-24 has been investigated by using variable-temperature IR spectroscopy with adsorbed isobutanol.

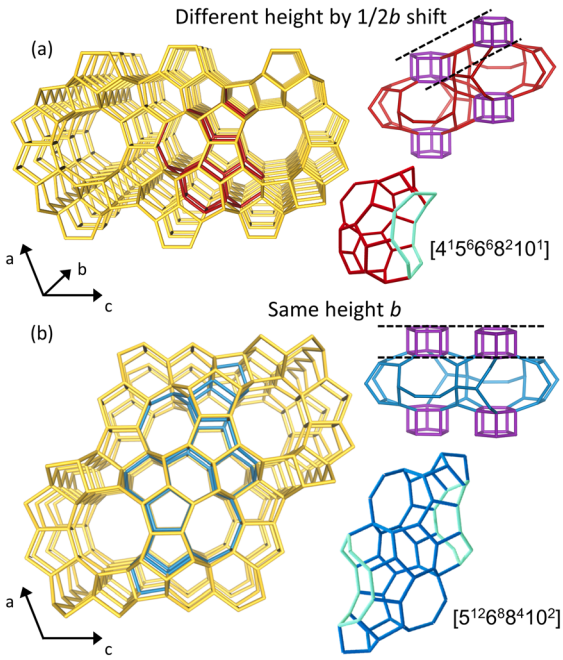

Fig. 1 Framework structures of polytypes (a) PST-24A and (b) PST-24C drawn from the two possible arrangements of d5r columns in the disordered medium-pore zeolite PST-24. Their 10-ring pocket, short 10-ring channel along [101] and d5r units are indicated in red, blue and purple, respectively. Only T–T connections, where T is Si or Al, are shown for clarity.

Experimental

Zeolite synthesis

The PMI^+-mediated synthesis of PST-24 under excess fluoride conditions was carried out using synthesis mixtures with the chemical composition $0.5PMIOH{\cdot}1.5HF{\cdot}xAl_2O_3{\cdot}1.0SiO_2{\cdot}5.0H_2O$, where x is varied between $0.01 \leq x \leq 0.2$. PMIOH was prepared and characterized as described in our recent report.[19] In a typical synthesis, aluminum hydroxide ($Al(OH)_3{\cdot}1.0H_2O$, Aldrich) was mixed with a solution of PMIOH and stirred at room temperature for 1 h. To this solution, a given amount of tetraethylorthosilicate (TEOS, 98%, Aldrich) was added and the mixture was stirred at room temperature for 3 h. The resulting mixture was heated at 80 °C to remove ethanol molecules generated by the hydrolysis of TEOS and some water to obtain the desired composition. If required, a small amount (4 wt% of the silica in the synthesis mixture) of seed crystals was added to the synthesis mixture. The seed crystals used here were calcined PST-24 with Si/Al = 200, which was previously synthesized using a synthesis mixture with Si/Al = 50 without using seed crystals. Then, an appropriate amount of HF (48% aqueous solution, J. T. Baker) was added while mixing with a spatula. The final synthesis mixture was transferred into a Teflon-lined 23 mL autoclave and heated under rotation (60 rpm) at 175 °C for 14 days. Ferrierite with Si/Al = 130 was synthesized using pyridine as an OSDA according to the procedures given elsewhere.[21]

As-made zeolites were calcined in air at 550 or 600 °C for 8 h to remove the occluded OSDAs and refluxed twice in 1.0 M NH_4NO_3 (2.0 g solid per 100 mL solution) for 6 h followed by calcination at 550 °C for 4 h in order to ensure that the zeolite was completely in its proton form. Two ZSM-5 zeolites with Si/Al = 47 and 95 and one ferrierite with Si/Al = 33 were obtained from Clariant and Tosoh, respectively, and converted to their proton form in a similar way described above. All zeolite catalysts studied here will be denoted by adding '(n)' to their common name, where n is the bulk Si/Al ratio.

Catalysis

Isobutanol dehydration was conducted under atmospheric pressure in a conventional continuous-flow microreactor. Before the experiments, each catalyst was pretreated under N_2 flow (50 mL min^{-1}) at 500 °C for 2 h and kept at the desired reaction temperature (200–250 °C) to stabilize the reactant/carrier gas distribution. A reactant stream of aqueous solution of isobutanol (99%, Alfa) containing 9 wt% of deionized water was then fed into the reactor containing 0.1 g of the catalyst at a weight hourly space velocity (WHSV) of 24.8 h^{-1}. The total gas flow at the reactor inlet was kept constant at 30 mL min^{-1}. The reaction products were analyzed online in a Varian CP-3800 gas chromatograph equipped with a CP-PoraPLOT Q capillary column (0.25 mm × 25 m) and a flame ionization detector, with the first analysis carried out after 10 min on stream. The isobutanol conversion was defined as the percentage of isobutanol consumed during the reaction, and the yield of a specific product *i* was calculated as the percentage of the amount of isobutanol converted to species *i*. The reusability test was carried out at 250 °C over the regenerated catalysts by calcination in air at 550 °C for 12 h.

Analytical methods

Powder X-ray diffraction (PXRD), elemental analysis by inductively coupled plasma (ICP) spectrometry, thermogravimetric and differential thermal analyses (TGA/DTA), scanning electron microscopy (SEM), N_2 sorption, ^{27}Al and ^{29}Si MAS NMR, NH_3 temperature-programmed desorption (TPD) and pyridine IR measurements were performed as described in our previous papers.[19,22] The ^{1}H–^{13}C CP MAS NMR spectra at a spinning rate of 15.0 kHz were recorded on a Bruker Avance III 500 HD spectrometer at a ^{13}C frequency of 125.770 MHz with a π/2 rad pulse length of 4.0 μs, a recycle delay of 60 s and an acquisition of *ca.* 4000 pulse transients. The ^{13}C chemical shifts are referenced relative to TMS.

Isobutanol adsorption–desorption and/or dehydration were monitored by variable-temperature IR spectroscopy. A self-supporting zeolite wafer of 13 mg (1.3 cm diameter) was activated at 450 °C under vacuum (10^{-3} Torr) for 2 h inside a home-built IR cell with CaF_2 windows, contacted with isobutanol vapor of 5.0 Torr at room temperature for 30 min, and evacuated at the same temperature under vacuum to a residual pressure of 10^{-3} Torr for another 30 min to remove physisorbed isobutanol. Then, the IR spectra were recorded on a Thermo-Nicolet 6700 FT-IR spectrometer with increasing temperature up to 300 °C, with a temperature interval of 5 °C and a holding time of 10 min at each temperature. The spectrum of gas-phase isobutanol was also recorded at room temperature and 5.0 Torr.

Results and discussion

Table 1 lists the representative products from PST-24 synthesis using PMI^+ as an OSDA and aluminosilicate mixtures but different Si/Al ratios (5–50) under excess fluoride conditions (HF/PMIOH = 3.0), both in the presence and absence of a small amount (4 wt% of the silica in the synthesis mixture) of H-PST-24 with Si/Al = 200 previously synthesized without adding any seed. Only products obtained from repeated synthesis runs are listed here. As recently reported,[19] we were not able to crystallize pure PST-24 from synthesis mixtures with Si/Al ratios lower than 50 in the absence of seed crystals. However, seeding allowed us to produce this medium-pore zeolite in its pure form from synthesis mixtures with Si/Al = 20 and 10, although both PST-24 zeolites are characterized by Si/Al ratios of *ca.* 50 that are still considerably higher than the ratios of their synthesis mixtures (Table 1). This suggests that there is a practical limit in Al incorporation into the PST-24 framework, further supported by the fact that SSZ-50 (RTH) was the phase formed at Si/Al = 7.5 and 5.0 even in the presence of PST-24 seed crystals.

Fig. 2 shows the PXRD patterns of H-PST-24(47) and H-PST-24(200) synthesized here. Comparison with the literature data reveals that both of them are phase-pure and highly crystalline,[19] as further evidenced by the N_2 micropore volumes in Table 2. The ^{27}Al MAS NMR spectra of their as-

Table 1 PMI^+-mediated PST-24 syntheses at different Si/Al ratios under excess fluoride conditions[a]

Si/Al ratio in the synthesis mixture	Addition of seeds[b]	Product[c]	Si/Al ratio in the product[d]
50	No	PST-24	200
50	Yes	PST-24	90
20	No	PST-24 + amorphous	
20	Yes	PST-24	53
10	No	SSZ-50 + amorphous	
10	Yes	PST-24	47
7.5	No	Amorphous + SSZ-50	
7.5	Yes	SSZ-50	
5.0	No	SSZ-50 + unknown	
5.0	Yes	SSZ-50	

[a] The composition of the synthesis mixture is $0.5PMIOH{\cdot}1.5HF{\cdot}xAl_2O_3{\cdot}1.0SiO_2{\cdot}5H_2O$, where x is varied between $0.01 \le x \le 0.2$. All syntheses were carried out under rotation (60 rpm) at 175 °C for 14 days. [b] A small amount (4 wt% of the silica in the synthesis mixture) of calcined PST-24 with Si/Al = 200 was added as seed crystals. [c] The phase appearing first is a major phase. [d] Determined by elemental analysis.

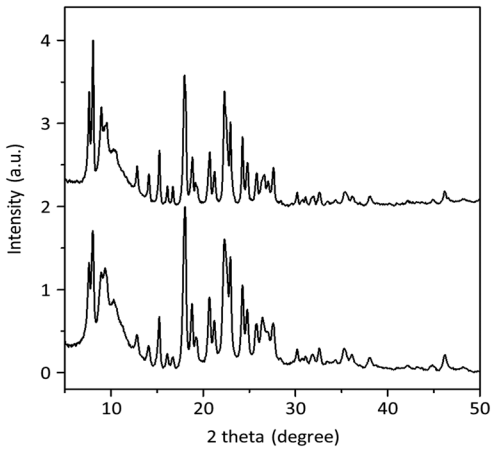

Fig. 2 PXRD patterns of H-PST-24(47) (bottom) and H-PST-24(200) (top).

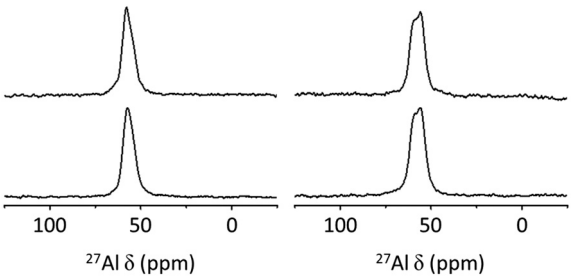

Fig. 3 ^{27}Al MAS NMR spectra of the as-made (left) and proton (right) forms of PST-24(47) (bottom) and PST-24(200) (top).

made and proton forms are compared in Fig. 3. Like those of the as-made form, the spectra of the proton form exhibited no noticeable ^{27}Al resonances around 0 ppm corresponding to extra-framework Al species, suggesting the high thermal stability of PST-24. However, this does not mean the complete lack of extra-framework Al species, because IR spectroscopy with adsorbed with pyridine indicates the presence of a non-negligible amount of Lewis acid sites in both H-PST-24(47) and H-PST-24(200) zeolites (Table 2) such as NMR-invisible Al in highly distorted extra-framework positions due to high quadrupolar coupling constant causing substantial signal broadening.[24] We also note that their ^{27}Al MAS NMR spectra show two resonances around 59 and 56 ppm in the tetrahedral Al region, but the spectra of their as-made form exhibit only one tetrahedral resonance around 58 ppm. It thus appears that upon OSDA removal, the eleven crystallographically distinct Al sites in the average structure of PST-24 are changed to two groups of Al sites with similar T–O–T angles. We speculate that interactions between the OSDA and the zeolite framework in as-made PST-24 would be strong enough to offset differences in the T–O–T angle of crystallographically distinct Al sites.

Fig. 4 shows the NH_3 TPD profiles of three pairs of H-PST-24, H-ZSM-5 and H-ferrierite zeolites with relatively low and high Si/Al ratios. All the TPD profiles of zeolites with low Si/Al ratios (*i.e.*, H-PST-24(47), H-ZSM-5(50) and H-ferrierite(33)) are characterized by two desorption peaks with maxima in the temperature ranges 280–330 and 410–440 °C, corresponding to NH_3 desorption from weak and strong acid sites, respectively. No significant differences in the NH_3 uptake (*i.e.*, the density of acid sites) were found (Table 2), in good agreement with the similarity in their Si/Al ratios. The same trend is observed for the profiles of three zeolites with higher Si/Al ratios, although there are no weak acid sites. Therefore, the catalytic results obtained from these three pairs of zeolites would reflect mainly the effects of the geometrical constraints imposed by each of the zeolite pore structures.

Fig. 5 shows isobutanol conversion and isobutene yield as a function of time on stream (TOS) in isobutanol dehydration at 250 °C and 24.8 h^{-1} isobutanol WHSV over six zeolite catalysts with different framework structures and/or Si/Al ratios. These catalytic data were obtained in the presence of 9% water vapor in order to check whether biomass-derived isobutanol can be directly used without further separation of concomitant water. We were not able to observe any noticeable amount of diisobutyl ether, a bimolecular dehydration product, over all zeolite catalysts studied, indicating that none of their pore structures are large enough to catalyze the S_N2-type dehydration of isobutanol.[25]

Table 2 Physicochemical properties of zeolite catalysts studied in this work

Catalyst ID[a]	Crystal shape and size[b] (μm)	N_2 BET surface area[c] (m^2 g^{-1})	Micropore volume[c] (cm^3 g^{-1})	Acidity[d] (μmol pyridine g^{-1})		NH_3 uptake[e] (mmol g^{-1})
				Brønsted	Lewis	
H-ZSM-5(50)	Spheres, 2.0–3.0	390	0.11	60	17	0.26
H-ZSM-5(95)	Spheres, 1.0–3.0	370	0.10	30	15	0.11
H-ferrierite(33)	Cuboids, 0.3–1.0	420	0.14	62	52	0.29
H-ferrierite(130)	Rectangular plates, 1.0 × 3.0 × 0.1	340	0.12	32	3	0.08
H-PST-24(47)	Aggregated rods, 0.05 × 0.5	410	0.13	47	39	0.26
H-PST-24(200)	Rectangular plates, 1.5 × 0.25 × 0.06	360	0.12	13	4	0.13

[a] The values in parenthesis are the bulk Si/Al ratios determined by elemental analysis. [b] Determined by SEM. [c] Calculated from N_2 adsorption data. [d] Determined from the intensities of the IR bands of retained pyridine at 1545 and 1455 cm^{-1} after desorption at 300 °C for 30 min, respectively.[23] [e] Determined from NH_3 TPD measurements.

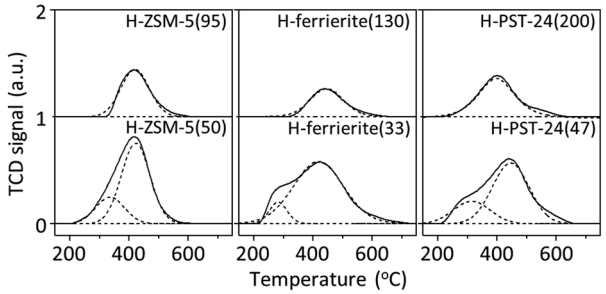

Fig. 4 NH_3 TPD profiles of three pairs of H-ZSM-5 (left), H-ferrierite (middle) and H-PST-24 (right) zeolites with low (bottom) and high (top) Si/Al ratios. Experimental and deconvoluted components are indicated by solid and dotted lines, respectively.

From the catalytic results in Fig. 5, it is clear that the initial isobutene yield, as well as the initial isobutanol conversion, is notably higher in the order H-ferrierite < H-ZSM-5 < H-PST-24, regardless of their Si/Al ratio. The excellent performance of H-PST-24 in isobutanol dehydration is further validated by the fact that the initial isobutene yield (61%) of H-PST-24(200) is considerably higher than the value (37%) of H-ZSM-5(50). This isobutene yield is even higher than that (52%) of phosphorus-modified ZSM-5 with a significantly higher Al content (Si/Al = 13) obtained at higher reaction temperature (280 *vs.* 250 °C) and a lower WHSV (7.4 *vs.* 24.8 h^{-1}) than our conditions.[17] We note that the initial isobutene yield and *n*-butenes/isobutene ratio (5.2% and 5.1 at conversion of 33%, respectively; Fig. 5) of H-ferrierite(33) are comparable to those (4.3% and 4.1 at conversion of 50%, respectively) of the same structure type of zeolite with a similar Si/Al ratio (28) at the same reaction temperature (250 °C) reported by Daele *et al.*,[16] imparting the reliability of our catalytic results. We also note that both the isobutanol conversion and isobutene yield of all H-ZSM-5 and H-ferrierite catalysts decrease with TOS and reach a steady state after 3 h on stream. However, this is not the case of H-PST-24(50) and H-PST-24(200) because their conversion and yield decrease gradually over the period of TOS studied here. For example, the isobutene yield (35%) of H-PST-24(47) at 10 h on stream is still twice higher than that (17%) of H-ZSM-5(50). It is worth noting that the activity loss of the zeolite catalysts would result from coke deposition, leading to a decrease in the number of accessible active sites rather than changes in the reaction mechanism or in the nature of active sites. This can be supported by the fact that a conversion decrease accompanied no changes in product selectivity.

Fig. 5 also compares selectivities to isobutene and *n*-butenes (*i.e.*, 1-butene, *trans*-2-butene and *cis*-2-butene) as a function of TOS in low-temperature isobutanol dehydration over all zeolite catalysts described above. It can be seen that while the initial isobutene selectivities (*ca.* 75%) of H-ZSM-5(50) and H-HZM-5(95) are higher by *ca.* 10% than those (61 and 66%, respectively) of H-PST-24 zeolites with similar Si/Al ratios, all of these four catalysts maintain almost constant isobutene selectivities over 10 h on stream. However, both H-

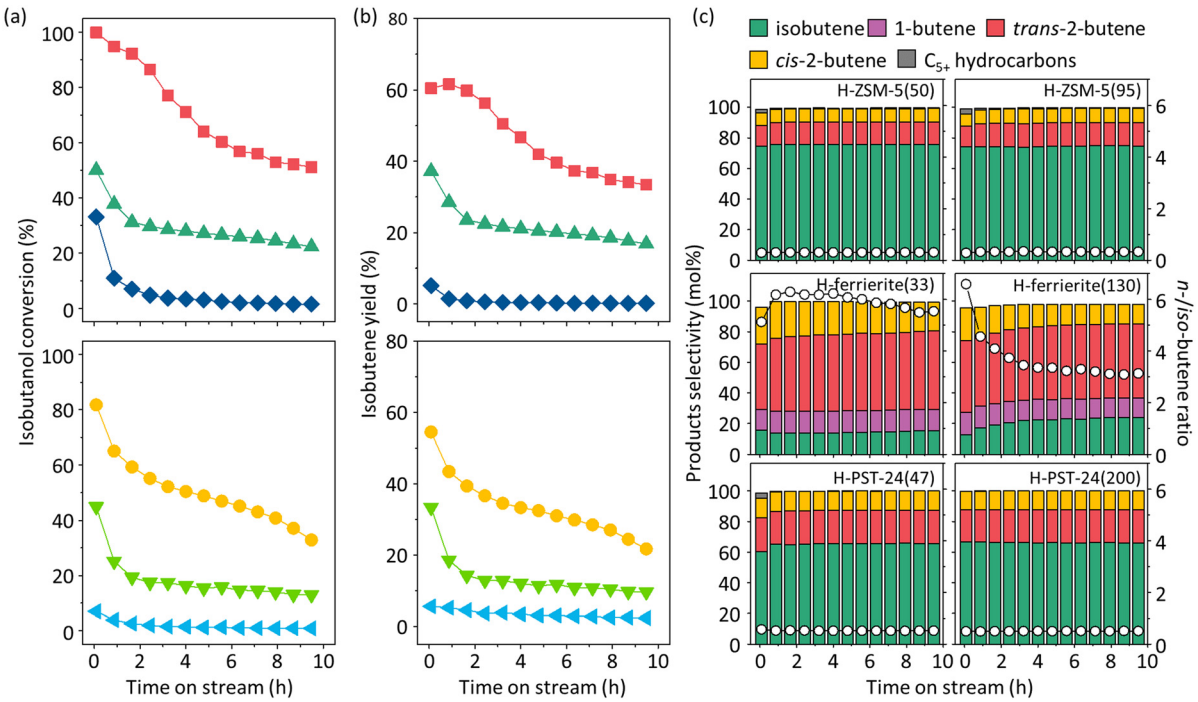

Fig. 5 (a) Isobutanol conversion, (b) isobutene yield and (c) selectivities to isobutene (green), 1-butene (purple), *trans*-2-butene (red), *cis*-2-butene (yellow) and hydrocarbons with more than 5 carbons (grey) as a function of TOS in isobutanol dehydration over H-ZSM-5, H-ferrierite and H-PST-24 catalysts with low (top) and high (bottom) Si/Al ratios at 250 °C and 24.8 h^{-1} isobutanol WHSV: H-ZSM-5(50), ▲; H-ZSM-5(95), ▼; H-ferrierite(33), ◆; H-ferrierite(130), ◀; H-PST-24(47), ■; H-PST-24(200), ●. The *n*-butenes/isobutene ratios in panel (c) are also given as open circles.

ferrierite(33) and H-ferrierite(130) were found to show much lower isobutene selectivities (≤23%) from the beginning of the reaction. In fact, they were characterized by much higher selectivities to *n*-butenes that should be a result of the isomerization of isobutylcarbenium cations to linear carbocations. This shows that H-ferrierite is structurally much less selective for low-temperature isobutanol dehydration than H-ZSM-5 and H-PST-24.

We next investigated the regenerability of H-ZSM-5(50) and H-PST-24(47), the two most representative catalysts in this study, by repeating the isobutanol dehydration run under the same reaction conditions as those described above, but over a longer period (30 h) of TOS. After each run, the used catalyst was regenerated by calcination at 550 °C in dry air for 8 h. The initial isobutene yield of H-ZSM-5(50) decreases to only *ca.* 15% of its fresh form after three regeneration cycles. As shown in Fig. 6, however, the yield of H-PST-24(47) is still over 80% of the fresh catalyst. Thermal analysis reveals that the amount (4.7 *vs.* 9.1 wt%) of organic species deposited during isobutanol dehydration at 250 °C for 30 h on stream is considerably higher in used H-ZSM-5(50) than in H-PST-24(47). Also, ^{1}H–^{13}C CP MAS NMR spectroscopy shows that used H-PST-24(47) gave no detectable resonances around 130 ppm due to the formation of hard aromatic coke (Fig. S1†), unlike used H-ZSM-5(50) and H-ferrierite(33), explaining its higher regenerability. However, because differences in the acidic properties of H-PST-24(47) and H-ZSM-5(50) are negligible (Table 2), it is still unclear what causes the formation of aliphatic coke only in this zeolite catalyst. One possible explanation is the unique pore structure of PST-24, although further study is necessary.

To understand why H-PST-24 is considerably more active for low-temperature isobutanol dehydration than H-ZSM-5 and H-ferrierite, we compared the IR spectra of H-ZSM-25(50), H-ferrierite(33) and H-PST-24(47) before and after isobutanol adsorption at room temperature. As shown in Fig. 7, isobutanol adsorption on these zeolites led to the appearance of two sharp bands at 2965–2968 and 2879–2882 cm^{-1} and one sharp band at 1472–1474 cm^{-1} that could be assigned to the C–H stretching and deformation modes of the molecules adsorbed on the zeolite Brønsted acid sites (BASs; bridging Si–OH–Al groups), respectively.[26] It should be noted that the intensities of IR bands from adsorbed isobutanol are much weaker on H-ferrierite(33) than on H-ZSM-5(50) and H-PST-24(47). Fig. 7 also shows that after isobutanol adsorption, the intensity of the BAS band around 3610 or 3600 cm^{-1} is again significantly weaker in the former zeolite than in the latter two zeolites. Therefore, we can conclude that the intracrystalline diffusion of isobutanol with a kinetic diameter of 5.4 Å (ref. 27) in ferrierite at room temperature is severely restricted, probably due to the small 10-ring size (4.2 × 5.4 Å) compared to ZSM-5 and PST-24.[19,28] As previously reported by Daele *et al.*,[16] in fact, the poor isobutene selectivity and yield of both H-ferrierite(33) and H-ferrierite(130) can be rationalized by considering that isobutanol dehydration occurs mostly on their external BASs.

It is also remarkable that the broad band around 3500 cm^{-1} in the spectrum of H-ZSM-5(50) assigned to internal Si–OH groups[29] migrates to 3260 cm^{-1} after isobutanol adsorption (Fig. 7), indicative of intermolecular hydrogen bonding. This suggests that isobutanol can be adsorbed on not only terminal Si–OH groups but also internal ones. We also carried out variable-temperature isobutanol-IR measurements on H-ZSM-5(50) and H-PST-24(47) and monitored the decrease in C–H stretching and C–H deformation band intensities of adsorbed isobutanol at

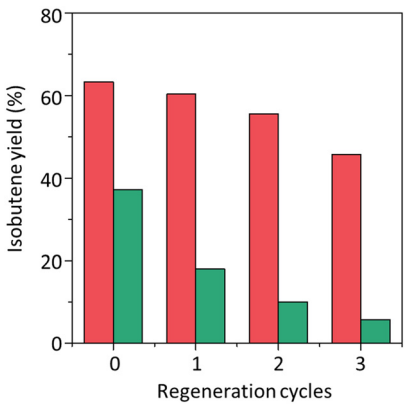

Fig. 6 Initial isobutene yield over H-ZSM-5(50) (green) and H-PST-24(47) (red) in four successive runs of isobutanol dehydration at 250 °C and 24.8 h^{-1} isobutanol WHSV for 30 h. Each catalyst was regenerated at 550 °C in dry air for 8 h prior to the next run. The reactant feed contains 9% H_2O vapor.

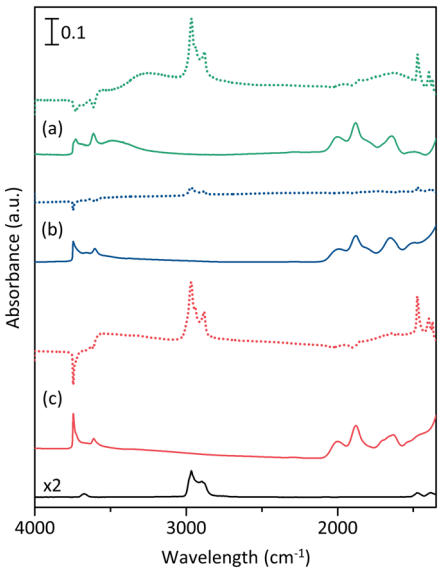

Fig. 7 IR spectra of (a) H-ZSM-5(50), (b) H-ferrierite(33) and (c) H-PST-24(47) before (solid line) and after (dotted lines) isobutanol adsorption at room temperature for 30 min. Prior to IR measurements on adsorbed isobutanol, each zeolite was evacuated at room temperature under vacuum to a residual pressure of 10^{-3} Torr for 30 min to remove physisorbed molecules. The bottom trace is the spectrum of gas-phase isobutanol.

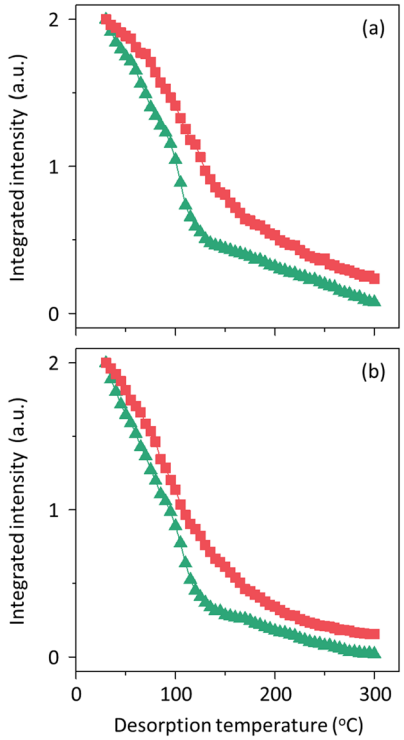

Fig. 8 Decrease in (a) C–H stretching and (b) C–H deformation vibration band intensities as a function of desorption temperature in the IR spectra of isobutanol adsorbed on H-ZSM-5(50) (▲) and H-PST-24(47) (■). Intensity normalization was made against the spectra measured at room temperature.

temperatures up to 300 °C (Fig. S2†). When normalized against the spectra obtained at room temperature, H-PST-24(47) was found to retain a relatively higher amount of isobutanol than H-ZSM-5(50) in the entire temperature range studied (Fig. 8). This indicates a stronger interaction of isobutanol with BASs in the former zeolite, partly explaining why H-PST-24(47) shows a considerably higher conversion in isobutanol dehydration at 250 °C than H-ZSM-5(50) (Fig. 5).

To better understand the pore structure effect of H-PST-24(47) and H-ZSM-5(50) on their isobutanol dehydration activity, we performed periodic density functional theory calculations using the exchange–correlation functional suggested by Perdew–Burke–Ernzerhof (PBE)[30] and with the additional empirical dispersion correction proposed by Grimme[31] implemented in the Vienna *ab initio* simulation package (VASP).[32] Unfortunately, the simultaneous alteration of both the transition state and intrazeolitic active site model did not allow us to capture the most energetically favorable transition state for this reaction, revealing unexpected complexity in calculations. Given the basic principle that catalytic conversion of reactant begins with its adsorption on the active sites of heterogeneous catalysts, on the other hand, it is not difficult to expect that the strong adsorption of reactants can lead to a high conversion as shown in Fig. 5, which is also the case of various oxygenated molecules.[33,34] Therefore, we speculate that the unique pore architecture of H-PST-24 rather than its acidic properties is mainly responsible for stronger isobutanol adsorption and thereby higher activity, making this zeolite an efficient catalyst for the dehydration of biomass-derived isobutanol.

Conclusions

We have successfully synthesized high Al-containing (Si/Al = 47) PST-24 zeolite *via* a seeding method and investigated its catalytic properties for low-temperature dehydration of isobutanol to isobutene. When compared to H-ZSM-5 and H-ferrierite with similar Si/Al ratios, H-PST-24 showed considerably higher activity and better catalyst stability. The overall characterization results strongly suggest that the excellent performance of this disordered medium-pore zeolite for isobutanol dehydration may be attributed mainly to its complex but unique pore structures. Further study, both experimental and theoretical, is necessary to better understand the origin of its catalytic activity.

Author contributions

Jeong Hwan Lee: conceptualization, data curation, formal analysis, investigation, methodology, writing – original draft, writing – review & editing. Donghui Jo: investigation, verification, writing – review & editing. Suk Bong Hong: conceptualization, data curation, supervision, project administration, verification, writing – review & editing.

Conflicts of interest

There are no conflicts to declare.

Acknowledgements

This work was supported by the National Creative Research Initiative Program (2012R1A3A3088711) through the National Research Foundation of Korea. We thank H. A. Aleksandrov and G. N. Vayssilov (University of Sofia) for the helpful discussion.

Notes and references

1 Emergen Research, **https://www.emergenresearch.com/industry-report/isobutene-market**, (accessed January 2024).
2 M. Mascal, *Biofuels, Bioprod. Biorefin.*, 2012, **6**, 483–493.
3 M. W. Peters and J. D. Taylor, *US Pat.*, 8373012, 2013.
4 C. Fu, Z. Li, C. Jia, W. Zhang, Y. Zhang, C. Yi and S. Xie, *Energy Convers. Manage.: X*, 2021, **10**, 100059.
5 D. E. Bryant and W. L. Kranich, *J. Catal.*, 1967, **8**, 8–13.
6 T. Tsuchida, T. Yoshioka, S. Sakuma, T. Takeguchi and W. Ueda, *Ind. Eng. Chem. Res.*, 2008, **47**, 1443–1452.
7 P. Kostestkyy, J. Yu, R. J. Gorte and G. Mpourmpakis, *Catal. Sci. Technol.*, 2014, **4**, 3861–3869.
8 K. Larmier, C. Chizallet, S. Maury, N. Cadran, J. Abboud, A.-F. Lamic-Humblot, E. Marceau and H. Lauron-Pernot, *Angew. Chem., Int. Ed.*, 2017, **56**, 230–234.

9 M. E. Potter, J. Amsler, L. Spiske, P. N. Plessow, T. Asare, M. Carravetta, R. Raja, P. A. Cox, F. Studt and L.-M. Armstrong, *ACS Catal.*, 2023, **13**, 5955–5968.
10 J. D. Taylor, M. M. Jenni and M. W. Peters, *Top. Catal.*, 2010, **53**, 1224–1230.
11 K. Tian, Q. Li, W. Jiang, X. Wang, S. Liu, Y. Zhao and G. Zhou, *RSC Adv.*, 2021, **11**, 11952–11958.
12 J.-L. Dubois, S. Segondy, G. Postole and A. Auroux, *Catal. Today*, 2023, **418**, 114126.
13 A. de Reviere, D. Gunst, M. K. Sabbe, M.-F. Reyniers and A. Verberckmoes, *Catal. Sci. Technol.*, 2021, **11**, 2540–2559.
14 H. H. Mooiweer, K. P. de Jong, B. Kraushaar-Czarnetzki, W. H. J. Stork and B. C. H. Krutzen, *Stud. Surf. Sci. Catal.*, 1994, **84**, 2327–2334.
15 Z. Buniazet, A. Cabiac, S. Maury, D. Bianchi and S. Loridant, *Appl. Catal., B*, 2019, **243**, 594–603.
16 S. V. Daele, D. Minoux, N. Nesterenko, S. Maury, V. Coupard, V. Valtchev, A. Travert and J.-P. Gilson, *Appl. Catal., B*, 2021, **284**, 119699.
17 C. Adam, D. Minoux, N. Nesterenko, S. V. Donk and J.-P. Dath, *US Pat.*, 9233885B2, 2016.
18 J. Shin, D. Jo and S. B. Hong, *Acc. Chem. Res.*, 2019, **52**, 1419–1427.
19 D. Jo, J. Zhao, J. Cho, J. H. Lee, Y. Liu, C.-J. Liu, X. Zou and S. B. Hong, *Angew. Chem., Int. Ed.*, 2020, **59**, 17691–17696.
20 T. Moteki and R. F. Lobo, *Chem. Mater.*, 2016, **28**, 638–649.
21 G. M. Pasquale and B. D. Murray, *US Pat.*, 5985238, 1999.
22 J. H. Lee, Y. J. Kim, T. Ryu, P. S. Kim, C. H. Kim and S. B. Hong, *Appl. Catal., B*, 2017, **200**, 428–438.
23 C. A. Emeis, *J. Catal.*, 1993, **141**, 347–354.
24 S. M. Maier, A. Jentys and J. A. Lercher, *J. Phys. Chem. C*, 2011, **115**, 8005–8013.
25 M. Kang, J. F. DeWilde and A. Bhan, *ACS Catal.*, 2015, **5**, 602–612.
26 J. N. Kondo and K. Domen, *J. Mol. Catal. A: Chem.*, 2003, **199**, 27–38.
27 K. Eum, K. C. Jayachandrababu, F. Rashidi, K. Zhang, J. Leisen, S. Graham, R. P. Lively, R. R. Chance, D. S. Sholl, C. W. Jones and S. Nair, *J. Am. Chem. Soc.*, 2015, **137**, 4191–4197.
28 C. Baerlocher and L. B. McCusker, Database of Zeolite Structures, **http://www.iza-structure.org/databases**, (accessed January 2024).
29 G. L. Woolery, L. B. Alemany, R. M. Dessau and A. W. Chester, *Zeolites*, 1986, **6**, 14–16.
30 J. P. Perdew, K. Burke and M. Ernzerhof, *Phys. Rev. Lett.*, 1996, **77**, 3865–3868.
31 S. J. Grimme, *J. Comput. Chem.*, 2006, **27**, 1787–1799.
32 G. Kresse and J. Hafner, *Phys. Rev. B: Condens. Matter Mater. Phys.*, 1994, **49**, 14251–14269.
33 T. Danuthai, S. Jongpatiwut, T. Rirksomboon, S. Osuwan and D. E. Resasco, *Appl. Catal., A*, 2009, **361**, 99–105.
34 T. D. Swift, H. Nguyen, Z. Erdman, J. S. Kruger, V. Nikolakis and D. G. Vlachos, *J. Catal.*, 2016, **333**, 149–161.